Nanoscale Res Lett (2008) 3:14–20
DOI 10.1007/s11671-007-9107-z

NANO EXPRESS

Synthesis and Characterization of Metal Nanoparticle Embedded Conducting Polymer–Polyoxometalate Composites

Pilli Satyananda Kishore · Balasubramanian Viswanathan · Thirukkallam Kanthadai Varadarajan

Received: 20 August 2007 / Accepted: 20 November 2007 / Published online: 13 December 2007

Abstract Phosphomolybdate has been employed simultaneously as the oxidizing agent for the monomer polymerization and the reduced polyoxometalate is used as reducing agent for the reduction of metal ions. The composites thus obtained have been characterized and may have many potential applications.

Keywords Conducting polymer · Polyoxometalates · Organic–inorganic hybrid nanocomposites · Silver · Gold

Introduction

The desire to synthesize nanostructures that combine the mechanical flexibility, optical and electrical properties of conducting polymers with the high electrical conductivity and magnetic properties of metal nanaoparticles has inspired the development of several techniques for the controlled fabrication of metal nanoparticle—conducting polymer composites. The incorporation of metal nanoparticles into the conducting polymer offers enhanced performance for both the host and the guest [1]. They have diverse application potentials in electronics because incorporation of metal clusters is known to increase the conductivity of the polymer [2]. The applications of these composites have also been extended to various fields such as, sensors [3, 4], photovoltaic cells [5], memory devices [6], protective coatings against corrosion [7], and supercapacitors [8]. Of particular interest is the application of these composites in catalysis. The polymer allows the control of the environment around the metal center, thus influencing selectivity of the chemical reactions. Polyaniline (PAni) supported Pd nanoparticles have been used for the oxidative coupling of the 2,6-di-*t*-butylphenol [9]. In terms of engineering applications, conducting polymer-supported metal nanoparticle catalysts are attractive materials for fuel cell design. For example, direct alcohol and proton exchange membrane fuel cell electrocatalysts based on conducting polymers have been studied [10–12]. Dispersing the metal nanoparticles into a conducting polymer matrix maintains the electrical connectivity of the particles to the underlying electrode [13, 14]. Under optimal conditions, this arrangement may result in enhanced electrocatalytic properties compared to the corresponding reactivity of the bulk metal [15]. Various methods for the preparation of nanoparticle embedded conducting polymer composites have been described, including template method for growing metal nanoparticles and polymers into nanostructures [16], photochemical preparation [17], and electrochemical methods involving, incorporation of metal nanoparticles during the electrosynthesis of the polymer [18] or electrodeposition of metal nanoparticles on preformed polymer electrodes [19], reduction of metal salts dissolved in a polymer matrix [20], and incorporation of preformed nanoparticles during polymerization of monomers [21] or nanoparticles generated during polymerization [22, 23]. Creation of ideal reaction conditions for the simultaneous reactions (polymerization and nanoparticle formation) is a challenge. The synthesis of nanoparticle and polymer using the same reagent in aqueous solution for generating nanoparticles and polymer in the form of a composite is particularly important, as it reduces the

P. S. Kishore · B. Viswanathan (✉) · T. K. Varadarajan
National Centre for Catalysis Research, Department of Chemistry, Indian Institute of Technology Madras, Chennai 600036, India
e-mail: bvnathan@iitm.ac.in

number of steps in a complex set of sequential reactions to the formation of a composite.

Polyoxometalates are well-defined metal-oxide polyanions that can undergo stepwise and multi-electron reactions while retaining structural integrity [24]. The introduction of polyoxometalates into conducting polymer network can be conveniently accomplished by taking advantage of the doping process of polymer leading to incorporation of charge-balancing species into the structure [25]. The strong oxidizing potential and acidic character of Keggin type polyoxometalate, Phosphomolybdic acid ($H_3PMo_{12}O_{40}$, PMo_{12}) provides perfect environment for the polymerization of monomers such as aniline, pyrrole, or thiophene to yield corresponding polymer–polyoxometalate composites. Different conducting polymers–polyoxometalate composites have been prepared by both chemical and electrochemical routes and used for photoelectrochemical and energy storage applications [26–29], but as such, there are no reports available on the incorporation of metal nanoparticles on the PAni-PMo_{12} composites by using a single reagent.

The present investigation focuses on the synthesis of Au or Ag nanoparticles embedded PAni-PMo_{12} composites (Ag-PAni-PMo_{12} and Au-PAni-PMo_{12}) and characterization of the formed composites. The PMo_{12} as reagent for simultaneous oxidation of aniline and reduction of metal salts for the synthesis of nanocomposites has not been reported so far. During the oxidation of aniline, PMo_{12} get reduced to heteropoly blue which then serve as reducing agent for the metal (Ag and Au) ions to form metal nanoparticles. The high-resolution transmission electron microscopic analysis revealed formation of metal embedded polymer nanostructures. The present method can also be extended for the preparation of various metal nanoparticles containing nanocomposites with different conducting polymers such as polypyrrole and poly(3,4-dioxy thiophene). Further, the properties of the inorganic–organic composites can be tailored by simply varying the polymer or polyoxometalate which are desired for electrocatalytic and sensor applications.

Experimental

Materials

Aniline from Aldrich was distilled under vacuum prior to use. Phophomolybdic acid ($H_3PMo_{12}O_{40}$, PMo_{12}) was procured from Aldrich and used further without purification. $AgNO_3$ and $HAuCl_4$ were obtained from Sisco research laboratories and used as received. Ultrasonic treatment of the composites was performed on TOSHCON sonicator (20 KHz, 100 W), India.

Preparation of Metal Nanoparticles Embedded PAni-PMo_{12} Composite

In a typical experiment, an aqueous solution of PMo_{12} (50 mM, 600 μL) was added to aniline monomer (100 μL) and this led to the reduction of PMo_{12} and oxidative polymerization of aniline. The appearance of an intense blue color due to the formation of polyoxomolybdate blue indicated the electron transfer from aniline to PMo_{12}. To this solution, 10 mM aqueous solution of $AgNO_3$ was added and ultrasonicated for 5 min. This was then allowed to stand for 24 h. The as prepared sample (Ag-PAni-PMo_{12}) was filtered out, washed, and dried under vacuum. Similar strategy was adopted for the preparation of Au nanoparticles by using 10 mM $HAuCl_4$ to prepare Au-PAni-PMo_{12} composite.

Structural Characterization

UV–Visible spectra were recorded on Cary 5E UV–Vis-NIR spectrometer. FTIR investigations were performed on Perkin–Elmer 1760 in the region 2,000–400 cm^{-1} with 32 scans by using KBr pellet mode. Powder X-ray diffraction patterns were recorded using a SHIMADZU XD-D1 diffractometer using a Ni-filtered Cu Kα radiation ($\lambda = 1.5418$ Å at a 0.2° scan rate (in 2θ). The morphology of the composites was investigated by a scanning electron microscopy (SEM) (FEI, Model: Quanta 200). The transmission electron micrograph (TEM) analysis was performed on CM12/STEM working at a 100 kV accelerating voltage. High-resolution transmission electron microscopy (HRTEM) was carried out on a JEOL-3010 instrument operating at 300 kV. Textural characteristics of composites were determined from nitrogen adsorption/desorption at 77 K using a Micrometrics ASAP 2020 instrument. The specific surface area, average pore diameters were determined. Prior to the measurements, the samples were degassed at 423 K. The BET specific surface area was calculated by using the standard Brunauer, Emmett, and Teller method on the basis of the adsorption data. The pore size distributions were calculated applying the Barrett–Joyner–Halenda (BJH) method. For conductivity measurements the composites were pressed in a manual hydraulic press at 750 MPa into a pellet of 13-mm diameter and 0.56-mm thickness. The conductivity measurements of Au-PAni-PMo_{12} and Ag-PAni-PMo_{12} were measured by the four-point Van der Pauw method [30]. The experimental setup included a Keithley 225 current source and Agilent 34401 voltmeter.

Results and Discussion

Polyoxometalates can be reduced in a plethora of ways, for example photochemically [31], through ^{60}Co-γ radiolysis [32], electrolytically [33], and with reductants [34]. The reduced polyoxometalate has served as reducing agent and stabilizing agent for the formation of various metal nanoparticle–polyoxometalate composites [35]. Gordeev et al. have noticed the ability of radiolytically two-electron reduced 12-tungstophosphate, $[PW_{12}O_{40}]^{5-}$, to reduce Ag ions into stable silver hydrosols [36]. The synthesis of metal nanoparticle–polyoxometalate composites based photo-catalytic reduction has been pioneered by Papaconstantinou et al. [31]. Wherein, polyoxometalates ($SiW_{12}O_{40}^{4-}$, $PW_{12}O_{40}^{3-}$) have served as photocatalysts and stabilizing agents for the formation of metal nanoparticles. Recently, Mandal et al. developed the synthesis of Au–Pd core shell nanoparticles using redox switching ability of Keggin ions [37]. In the present work, the formation of reduced PMo_{12} was observed during the polymerization of aniline in the presence of PMo_{12}. The reduced PMo_{12} species served as reducing agent for the reduction of metal ions to form metal nanoparticle embedded PAni-PMo_{12} composite. The different stages of synthesis of the composites (Steps I and II, Scheme 1) were monitored by UV–Vis spectra (Fig. 1). Figure 1a corresponds to the UV–Vis spectrum recorded from PMo_{12} solution which has no obvious absorbance in the range 400–800 nm. Figure 1b corresponds to the UV–Vis absorption of the blue-colored solution containing PMo_{12} and aniline (Step I, Scheme 1); the presence of an absorption band at 700 nm can be seen and is characteristic of one-electron reduced PMo_{12} (electron is transferred from aniline to PMo_{12}). The produced d^1 metal ion [38] of Mo is responsible for the d–d transition resulting in absorption in the visible region. Figure 1c, d correspond to the spectra of PMo_{12}-PAni solution to which $AgNO_3$ and $HAuCl_4$ solutions were added respectively (Step II, Scheme 1); strong absorption bands at 450 and 573 nm due to the excitation of surface plasmon resonance of Ag and Au nanoparticle in Ag-PAni-PMo_{12} (Fig. 1c) and Au-PAni-PMo_{12} (Fig. 1d), respectively, were observed.

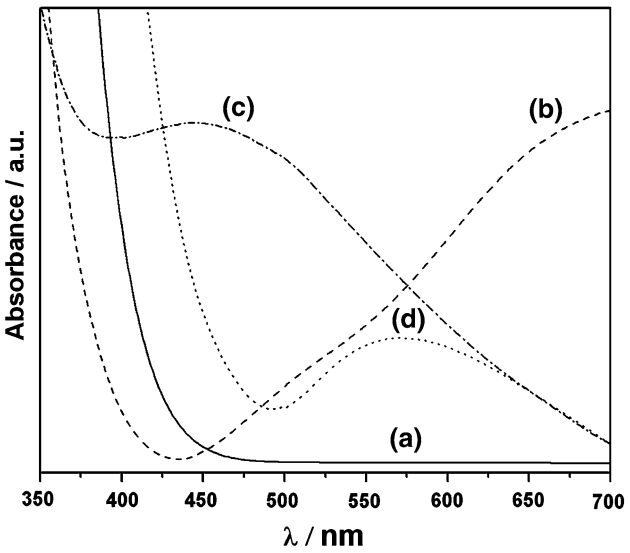

Fig. 1 UV–Vis spectra of (**a**) 10 mM PMo_{12} (**b**) a mixture of 5 mM PMo_{12} and 20 μL of aniline (**c**) after addition of 10 mM $AgNO_3$ (**d**) after addition of 10 mM $HAuCl_4$

The presence of Ag and Au nanoparticles in Ag-PAni-PMo_{12} and Au-PAni-PMo_{12} was further confirmed by powder XRD measurements, as shown in Fig. 2. The XRD pattern of Ag nanoparticles containing composite showed four strong peaks with maximum intensity at 38.1°, 44.3°, 64.4°, and 77.4° representing Bragg's reflections from (111), (200), (220), and (311) planes of the standard cubic phase of Ag (Fig. 2a). Au-PAni-PMo_{12} composite also exhibited the presence of four strong peaks with maximum intensity at 38.2°, 44.4°, 64.5°, and 77.5° representing (111), (200), (220), and (311) planes of standard cubic phase of Au (Fig. 2b).

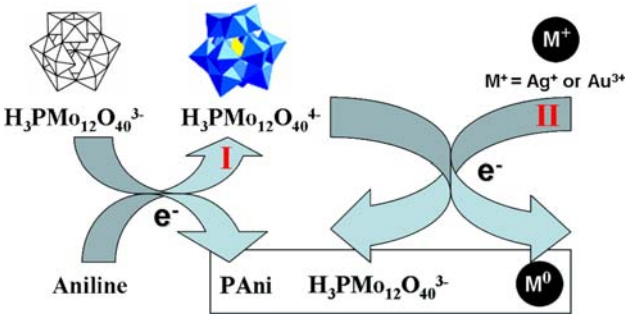

Scheme 1 Schematic representation of the PMo_{12}-mediated synthesis of metal nanoparticle embedded PAni-PMo_{12} composites

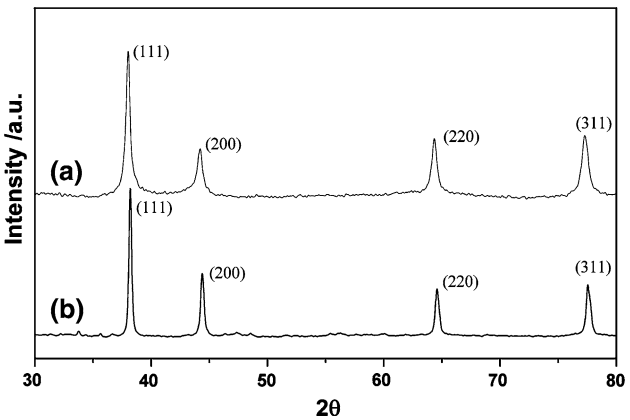

Fig. 2 XRD patterns of (**a**) Ag-PAni-PMo_{12} and (**b**) Au-PAni-PMo_{12}

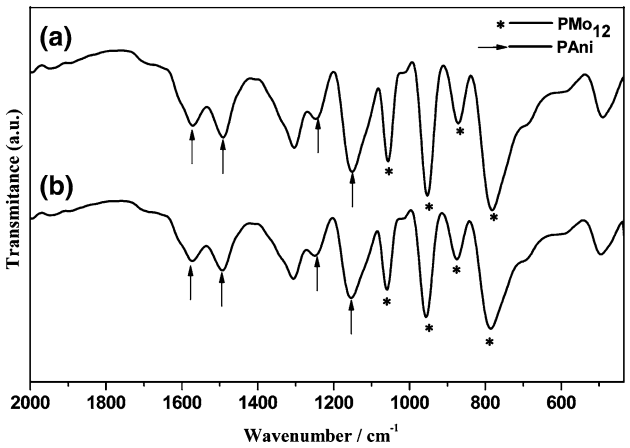

Fig. 3 FTIR spectra of (**a**) Ag-PAni-PMo_{12} and (**b**) Au-PAni-PMo_{12}

In order to confirm the presence of PAni and the phosphomolybdate anion in the composites, Fourier transform infrared (FTIR) analysis of the Ag-PAni-PMo_{12} and Au-PAni-PMo_{12} (Fig. 3a, b) nanocomposites was carried out. Both the composites showed the characteristic bands of PAni (marked with arrows) and phosphomolydate anion (marked with circles). The peak at 1,575 cm^{-1} is assigned to a deformation mode of benzene rings, the one at 1,488 cm^{-1} to a deformation of benzene or quinoide rings, the one at 1,248 and 1,147 cm^{-1} to a C=N stretching of a secondary amine, at 1,060 cm^{-1} to a P–O bond, at 955 cm^{-1} to a Mo=O terminal bond, at 876 cm^{-1} to a vertex Mo–O–Mo bond, and finally at 800 cm^{-1} to an edge Mo–O–Mo bond.

The nitrogen adsorption/desorption isotherms of Ag-PAni-PMo_{12} and Au-PAni-PMo_{12} composites are shown in Fig. 4a, b respectively. The isotherms were identified as type IV isotherms with H3 type Hysteresis loops. The pore size distributions were calculated and represented in the insets of Fig. 4a, b. Both the composites exhibited a broad distribution of mesopores ranging from 2 nm to 43 nm. The average pore sizes were determined and found to be 23.8 nm for Au-PAni-PMo_{12} and 22.4 nm for Ag-PAni-PMo_{12}. The BET surface areas were also found to be similar, 7 and 6 m^2/g for Ag-PAni-PMo_{12} and Au-PAni-PMo_{12} composites respectively.

The morphology of the prepared nanocomposites was examined using scanning electron microscopy (SEM). Figure 5a, b shows the SEM images of Ag-PAni-PMo_{12} and Au-PAni-PMo_{12} composites, respectively. The nanocomposites exhibited a highly mesoporous structure which is of great interest for their application as electrodes since it represents an optimization of the electrode–electrolyte interface.

Figure 6a, b shows typical low-magnification TEM images of the Ag-PAni-PMo_{12} composites. The spherical Ag nanoparticles are well distributed and stabilized by the polymer. The corresponding histogram (Fig. 7a) of the size distribution of the Ag nanoparticles indicates a broad distribution ranging from 3.5 nm to 9 nm of the Ag nanoparticles formed during the reaction. TEM images of Au-PAni-PMo_{12} composite (Fig. 6c, d) show most of the Au nanoparticles aggregated with a size distribution ranging from 4 nm to 9 nm (Fig. 7b). The particles are aggregated into dendritic structures composed of nanorod arms with an average diameter of ca 3 nm and length 10 nm and they were rather polydisperse. The detailed structure of the Ag and Au nanoparticles in the prepared nanocomposites was further revealed by high-resolution TEM (Fig. 8). From Fig. 8a, it can be seen that the spherical silver nanoparticles embedded in PAni polymer in the Ag-PAni-PMo_{12} composite and nanoparticles have

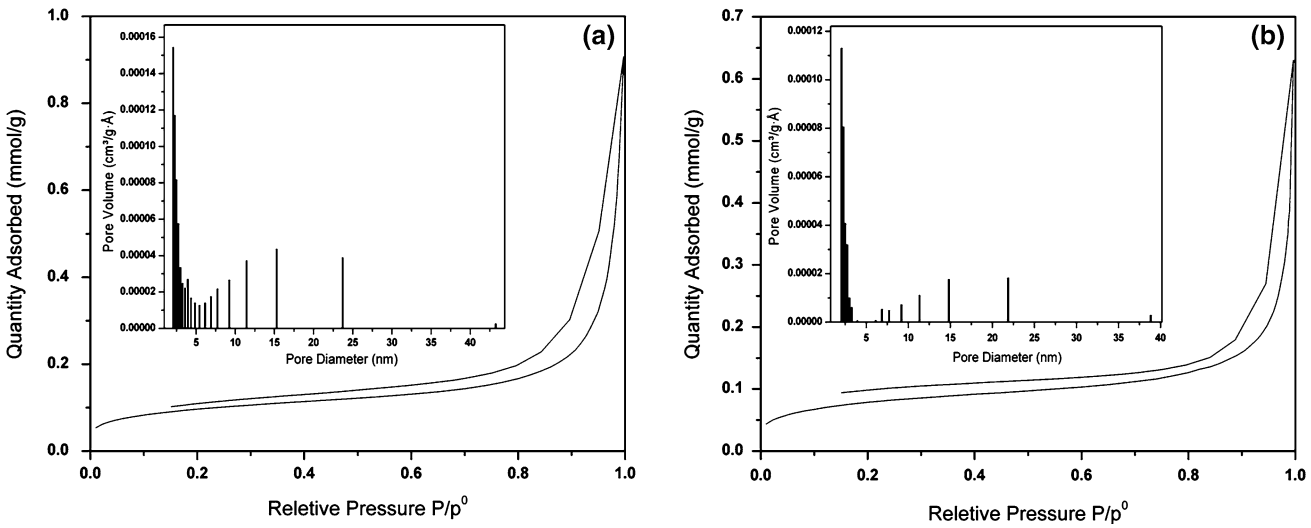

Fig. 4 N_2 adsorption/desorption isotherms of (**a**) Ag-PAni-PMo_{12} and (**b**) Au-PAni-PMo_{12} (inset: the BJH pore size distribution)

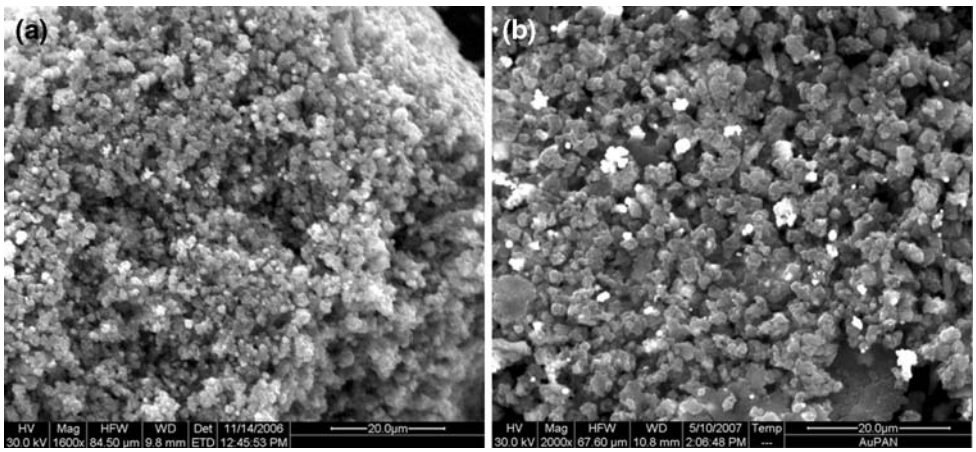

Fig. 5 SEM images of (**a**) Ag-PAni-PMo_{12} and (**b**) Au-PAni-PMo_{12}

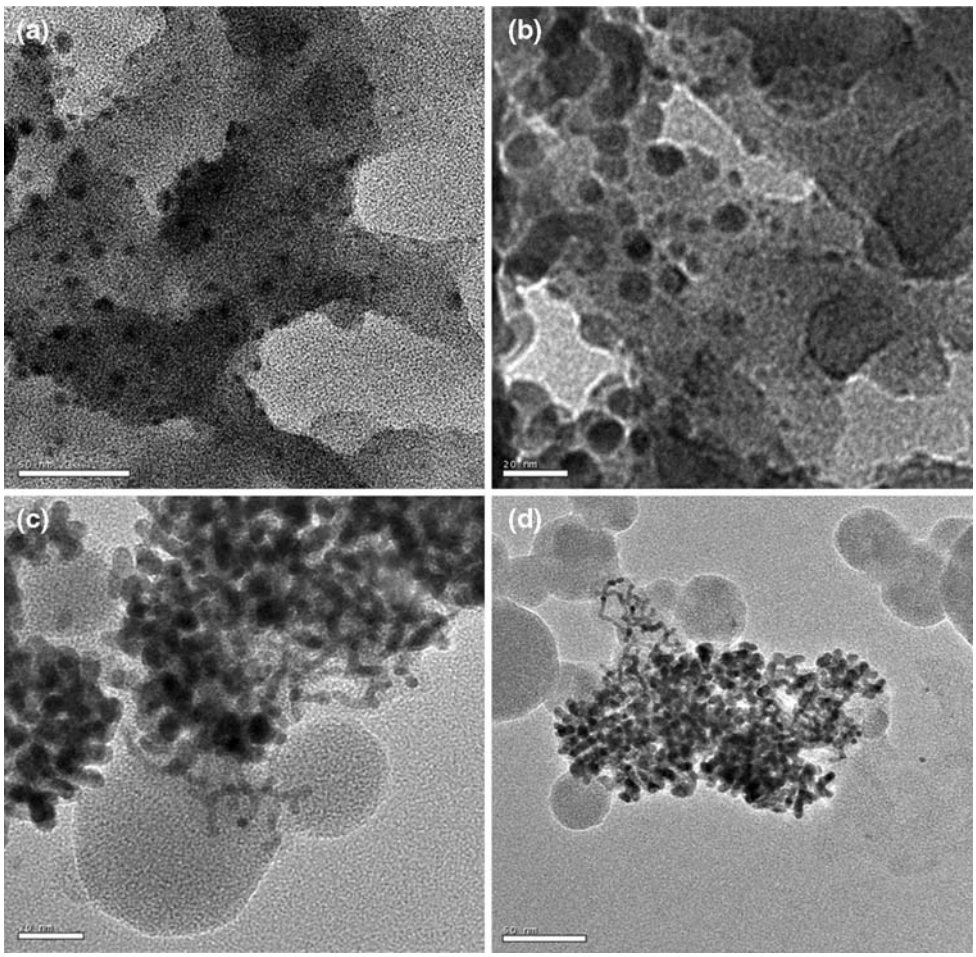

Fig. 6 TEM images of (**a**) & (**b**) Ag-PAni-PMo_{12} and (**c**) & (**d**) Au-PAni-PMo_{12}

clear crystalline planes aligned along a specific direction with a d spacing of 2.36 Å. Figure 8b indicated the dark Au nanorod arms surrounded by a grayish sheath of PAni in the Au-PAni-PMo_{12} composite. The planes of the rods are aligned with a d spacing of 2.38 Å. The electrical conductivities of the Ag-PAni-PMo_{12} and Au-PAni-PMo_{12} composites measured with a four-probe technique were found to be 12.5 and 6.5 S cm^{-1}, respectively.

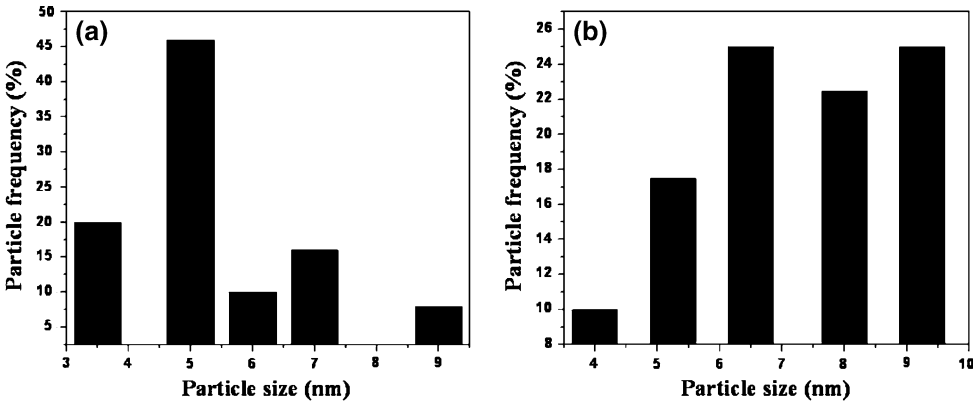

Fig. 7 Particle size distribution of (**a**) Ag-PAni-PMo_{12} and (**b**) Au-PAni-PMo_{12}

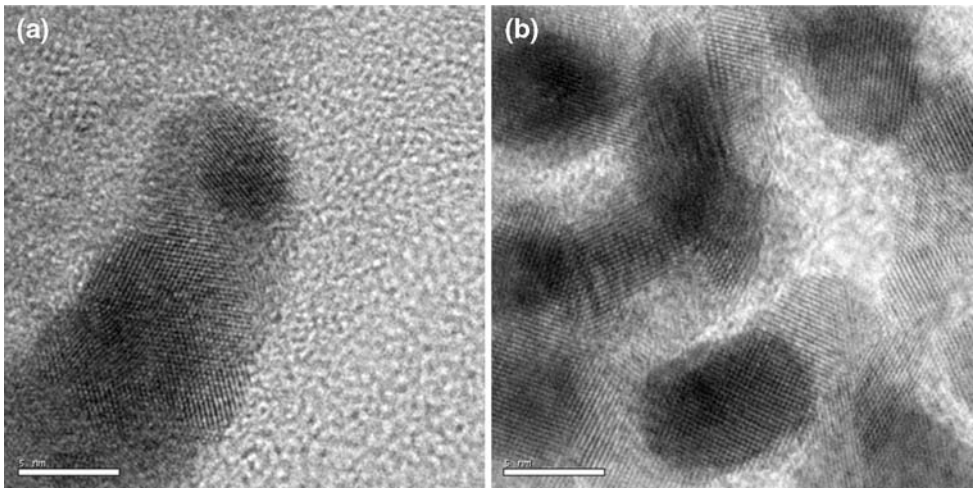

Fig. 8 HRTEM images of (**a**) Ag-PAni-PMo_{12} and (**b**) Au-PAni-PMo_{12}

Conclusions

In conclusion, a simple method has been introduced to prepare Ag and Au nanoparticle containing organic–inorganic nanocomposites of PAni and PMo_{12} using the excellent electron transfer capability of polyoxometalates. PMo_{12} has served dual role in the formation of the nanocomposites; it served as oxidizing agent for the polymerization of aniline and reducing agent for the formation of metal nanoparticles. In particular, the synthesized nanocomposites exhibited embedded metal nanoparticles in the polymer matrix. Furthermore, the method can be extended to the synthesis of other conducting polymers and opens up a new route to prepare inorganic–organic nanocomposites with wide variation of properties. It should also stimulate the exploration of applications of these nanocomposites especially in fields such as sensors, catalysis, and composite materials.

References

1. R. Gangopadhyay, A. De, Chem. Mater. **12**, 608 (2000)
2. Z. Peng, L. Guo, Z. Zhang, B. Tesche, T. Wilke, D. Ogermann, S. Hu, K. Kleinermanns, Langmuir **22**, 10915 (2006)
3. Y. Xian, Y. Hu, F. Liu, Y. Xian, H. Wang, L. Jin, Biosens. Bioelectron. **21**, 1996 (2006)
4. A.A. Athawale, S.V. Bhagawat, P.P. Katre, Sens. Actuators, B Chem. **114**, 263 (2006)
5. W.U. Huynh, J.J. Dittmer, A.P. Alivisatos, Science **295**, 2425 (2002)
6. R.J. Tseng, J. Huang, J. Ouyang, R.B. Kaner, Y. Yang, Nano. Lett. **5**, 1077 (2005)
7. M.A. Malik, M.T. Galkowski, H. Bala, B. Grzybowska, P.J. Kulesza, Electrochim. Acta. **44**, 2157 (1999)
8. C.C. Hu, E. Chen, J.Y. Lin, Electrochim. Acta. **47**, 2741 (2002)
9. T. Amaya, D. Saio, T. Hirao, Tetrahedron Lett. **48**, 2729 (2007)
10. B. Rajesh, P. Zelenay, Nature **443**, 63 (2006)
11. B. Rajesh, K.R. Thampi, J.M. Bonard, A.J.M. Evoy, N. Xanthopoulos, H.J. Mathieu, B. Viswanathan, J. Power Sources **133**, 155 (2004)
12. B. Rajesh, K.R. Thampi, J.M. Bonard, H.J. Mathieu, N. Xanthopoulos, B. Viswanathan, J. Power Sources **141**, 35 (2005)
13. E. Granot, E. Katz, B. Basnar, I. Willner, Chem. Mater. **17**, 4600 (2005)
14. S. Tian, J. Liu, T. Zhu, W. Knoll, Chem. Mater. **16**, 4103 (2004)
15. A.A. Mikhaylova, E.B. Molodkina, O.A. Khazova, V.S. Bagotzky, J. Electroanal. Chem. **509**, 119 (2001)
16. S.M. Marinakos, D.A. Shultz, D.L. Feldheim, Adv. Mater. **11**, 34 (1999)
17. A. Marc, G.Y. Breimer, S. Sheldon, A.S. Omowunmi, Nano Lett. **1**, 305 (2001)
18. H.H. Zhou, X.H. Ning, S.L. Li, J.H. Chen, Y.F. Kuang, Thin Solid Films **510**, 164 (2006)

19. D.W. Hatchett, M. Josowicz, J. Janata, Chem. Mater. **11**, 2989 (1999)
20. S.T. Selvan, J.P. Spatz, H.A. Klok, Adv. Mater. **10**, 132 (1998)
21. M.M. Oliveira, E.G. Castro, C.D. Canestraro, D. Zanchet, D. Ugarte, L.S. Roman, A.J.G. Zarbin, J. Phys. Chem. B. **110**, 17063 (2006)
22. A. Chen, H. Wang, X. Li, Chem. Commun. 1863 (2005)
23. T.S. Sarma, D. Chowdhury, A. Paul, A. Chattopadhyay, Chem Commun. 1048 (2002)
24. E. Papaconstantinou, Chem. Soc. Rev. **18**, 1 (1989)
25. G. Bidan, M. Lapkowski, J.P. Travers, Synth. Metals **28**, C113 (1989)
26. P.G. Romero, N.C. Pastor, M.L. Cantu, Solid State Ionics **101–103**, 875 (1997)
27. M.L. Cantu, P.G. Romero, Chem. Mater. **10**, 698 (1998)
28. J. Vaillant, M.L. Cantu, K.C. Gallegos, N.C. Pastor, P.G. Romero, Prog. Solid State. Chem. **34**, 147 (2006)
29. L. Adamczyk, P.J. Kulesza, K. Miecznikowski, B. Palys, M. Chojak, D. Krawczyk, J. Elecrochem. Soc. **152**, E98 (2005)
30. L.J. Van der Pauw, Philips Res. Rep. **13**, 1 (1958)
31. A. Troupis, A. Hiskia, E. Papaconstantinou, Angew. Chem. Int. Ed. **41**, 1911 (2002)
32. E. Papaconstantinou, J. Chem. Soc. Faraday Trans. **78**, 2769 (1982)
33. I.A. Weinstock, Chem. Rev. **98**, 113 (1998)
34. A. Muller, S.Q.N. Shah, H.B.M. Schmidtmann, Nature **397**, 48 (1999)
35. V. Kogan, Z. Aizenshtat, R.P. Biro, R. Neumann, Org. Lett. **4**, 3529 (2002)
36. A.V. Gordeev, B.G. Ershov, High Energ. Chem. **33**, 218 (1999)
37. S. Mandal, A.B. Mandale, M. Sastry, J. Mater. Chem. **14**, 2868 (2004)
38. M. Verga, E. Papaconstantinou, M.T. Pope, Inorg. Chem. **9**, 662 (1970)